Volume 1 | Number 1 | Jan 2013 | Pages 1–100

Journal of
Materials Chemistry A

Materials for energy and sustainability
www.rsc.org/materialsA

ROYAL SOCIETY
OF CHEMISTRY

ROYAL SOCIETY
OF **CHEMISTRY**

www.rsc.org/materialsA

Journal Name

Journal of Materials Chemistry A

ARTICLE TYPE

Synthesis of three-dimensional hyperbranched TiO2 nanowire arrays with significantly enhanced photoelectrochemical hydrogen production

Zhenghui Pan,[a,b,+] Yongcai Qiu,[b,+] Jie Yang,[a] Meinan Liu,[b] Lisha Zhou,[b] Yijun Xu,[b] Leimei Sheng,[a] Xinluo Zhao*[a], and Yuegang Zhang*[b]

Three-dimensional (3D) hierarchical nanostructure is one of the promising candidates for high performance photoelectrochemical (PEC) water splitting electrode due to the reduced carrier diffusion distance, improved light absorption efficiency and charge collection efficiency. Here, by growing omnidirectional, densely-packed branches on TiO2 nanowires, we demonstrated a 3D hyperbranched hierarchical TiO2 nanowire (HHNW) architecture that could significantly enhance the performance of PEC water splitting. Under a solar simulator with chopped AM 1.5G light of 100 mW cm^{-2} intensity, the HHNW electrode yielded a photocurrent density of 1.21 mA cm^{-2} at 1.23 V with respect to the reversible hydrogen electrode (RHE), which was about four times higher than that of TiO2 nanowires (NWs) (0.34 mA cm^{-2}). The highest incident photon-to-current conversion efficiencies (IPCE) obtained from our HHNWs was 77% at 365−425 nm. This greatly improved PEC performance can be attributed to the improved light absorption efficiency and the increased contact surface areas at the TiO2/electrolyte interface.

Photoelectrochemical (PEC) water splitting is one of the efficient ways to convert sunlight to the cleanest fuel --- hydrogen. The development of photoelectrode materials with a suitable bandgap for efficient light harvesting and fast water oxidation is one of the key challenges for PEC water splitting.[1-10] Since the pioneering work of the practical PEC water splitting using n-type TiO2 was reported by Honda and Fujishima in 1972,[11] various metal oxide semiconductors,[12-19] including TiO2,[12-14] ZnO,[15-17] α-Fe2O3,[18] WO3,[19] and composited semiconductors[20] have been investigated as photoanodes for PEC water splitting. Among all these photoelectrodes, TiO2 has been attracted the most attention due to its excellent photocatalytic activity, appropriate band edge positions, high photochemical stability, low cost and non-toxicity. The conventional TiO2 photoanode is in the form of nanoparticle (NP) based film because of its large surface area to volume ratio.[12,21] However, the photo-induced electrons suffer serious recombination at the interfaces in the NP based films where the electron diffusion is slow.[22] Due to the significant electron trapping at grain boundaries, the electron diffusion coefficient of these NP based films is several orders of magnitude lower than that in one-dimensional (1D) TiO2 nanostructures.[23] 1D nanostructures can also decouple the directions of light absorption and provide a direct electron transport pathway for

these semiconductor arrays to conductive substrates, thus reducing the carrier diffusion length and improving the charge collection efficiency. Therefore, much effort has been focused on 1D nanostructured metal oxide arrays grown on conductive substrates such as nanowires (NWs)[24-25] and nanotubes (NTs).[26-27] The 1D architectures made of NWs and NTs usually have a relatively low surface area and contain a large volume of free space within them. To further improve PEC device performance, it is highly desirable to synthesize three-dimensional (3D) hierarchical TiO2 nanostructures,[28-29] such as nanobranches[6, 30-32] and nanoflowers,[33-36] for improving light harvesting efficiency and enhancing contact surface areas at TiO2/electrolyte interface. Nevertheless, most of the demonstrated 1D nanostructures have either sparsely or tiny distributed branches, normally possess a lower internal surface area than the conventional 20 nm nanoparticle counterpart, leaving much room for improvement.

In this paper, we report on the preparation of a 3D hyperbranched hierarchical TiO2 nanowire (HHNW) array as a model photoanode for efficient PEC water splitting. The HHNWs maintain an efficient electron transport almost as good as TiO2 NWs, but have improved light absorption and increased contact surface areas between electrode materials and electrolytes due to their omnidirectional, densely-packed hyperbranched nanostructure. The designed advantage of the HHNW structure has been demonstrated by its measured photocurrent density of 1.21 mA cm^{-2} at an applied bias of 1.23 V vs. RHE, which is much higher than those of NWs (0.34 mA cm^{-2}) and hierarchical TiO2 nanowires (HNWs) electrode (0.75 mA cm^{-2}).

Experimental Section

Chemicals. Fluorine-doped tin oxide (1.5 × 2 cm); Titanium tetrachloride (99.9%. Aladdin); hydrochloric acid (36.0–38.0 wt%, Sinopharm Chemical Regent Co., Ltd); Titanium trichloride solution (20 wt% of TiCl3 in H2O and HCl solution, Sinopharm Chemical Regent Co., Ltd). All reagents were used directly without any further purification.

Preparation of aligned TiO2 nanowires (NWs). TiO2 NWs were synthesized directly on fluorine-doped tin oxide (FTO) substrates by a modified hydrothermal method according to a previous report.[23] In a typical synthesis process, FTO substrates (1.5 × 2 cm) were ultrasonically cleaned in acetone, ethanol and deionized (DI) water each for 15 min and then dried in air. As a precursor solution, 0.25 ml of Titanium tetrachloride (TiCl4) was slowly added into a mixture solution of 30 mL of hydrochloric acid

aqueous solution (36.0–38.0 wt%) and 30 ml of DI water, followed by magnetically stirring for 30 min. Two pieces of FTO substrates were fixed on a home-made Teflon-socket at an angle against the horizontal plane with their conductive sides facing down. Then the Teflon-socket and the hydrothermal solution were transferred into a sealed Teflon-lined stainless steel reactor, which was then placed in an electric oven and hydrothermal treatment was conducted at 150 $^\circ$C for 6 h. After the reaction was completed and the autoclave was cooled down to room temperature, the as-prepared sample was taken out and rinsed extensively with ethanol, DI water and dried at room temperature.

Preparation of hierarchical TiO$_2$ nanowires (HNWs). A two-step procedure was employed for synthesis of hierarchical TiO$_2$ NWs. The as-prepared NWs form the above process were firstly immersed in a high concentration (0.4 M) TiCl$_4$ aqueous solution and kept at 100 $^\circ$C for 1 h to obtain densely seeded surface. Then these seeded NWs were immersed into the same solution as described in the preparation of aligned TiO$_2$ nanowires for further hydrothermal treatment of 3 h to grow HNWs.

Preparation of 3D hyperbranched hierarchical TiO$_2$ nanowires (HHNWs). For synthesis of the omnidirectional densely-packed hyperbranched nanostructure, HNWs were annealed in air at 450 $^\circ$C for 30 min, then immersed in an aqueous solution consisting of 10 mL of DI water, 0.3 mL of HCl, and 0.15 mL of TiCl$_3$ solution (20 wt% of TiCl$_3$ in H$_2$O and HCl solution) in a Pyrex glass bottle, and finally kept at 80 $^\circ$C for 2 h in an oven. The as-prepared samples were thoroughly washed with DI water followed by ethanol, and subsequently annealed at 450 $^\circ$C for 1 h in air.

Material characterization. The microstructure of samples was characterized by a Quanta 400 FEG field-emission scanning electron microscope (FE-SEM) and a Tecnai G2 F20 S-Twin field-emission transmission electron microscope (FE-TEM); X-ray diffraction (XRD) was used to study the crystal structure of the samples with a Bruker D8 diffractometer; The Raman spectra was also used to analyze the structure information of the as-obtained samples with a LabRAM HR evolution Raman spectrometer; Diffused reflectance spectra was collected on the samples using a Perkin-Elmer UV/vis spectrophotometer (model Lambda 20); The light source (Oriel solar simulator, 450 W Xe lamp, AM 1.5 global filter) was calibrated to 1 sun (100 mW cm^{-2}) using an optical power meter (Newport, model 1916-C) equipped with a Newport 818P thermopile detector. The electrochemical data were collected by using Zahner Zennium C-IMPS system.

Photoelectrochemical performance test. NWs, HNWs, and HHNWs were used as the working electrode; A Pt net was served as the counter electrode; and a Ag/AgCl was used as the reference electrode. The reversible hydrogen electrode (RHE) calculation was based on the equation, E(RHE) = E(Ag/AgCl) + 0.1976 V + 0.059 pH). All three electrodes were immersed in a quartz electrolytic cell; the photoelectrode was covered by ethoxyline except for a window for light illumination. N$_2$ gas was purged through the cell during the measurement to instantaneously flush away O$_2$ from the working electrode and H$_2$ from the counter electrode.

Results and discussions

A schematic illustration of the fabrication process of the HHNWs structure is shown in Fig. 1. The as-obtained structures were characterized after each step of growth by FE-SEM. As shown in
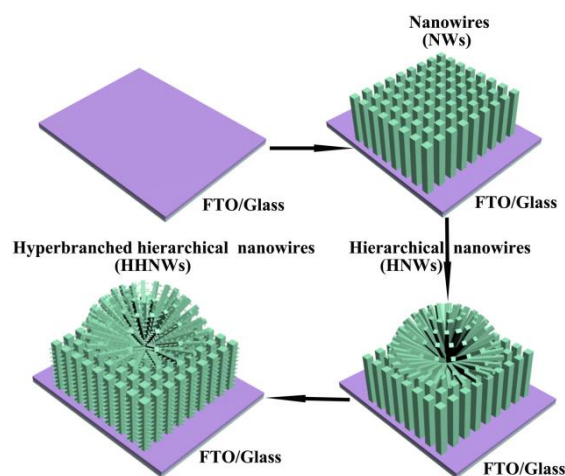

Figure 1. Schematic illustration of the fabrication process of the HHNWs structure.

Fig. 2a, the NWs after the first growth step have an average diameter of around 150 nm and the coverage density is evaluated to be around 6.0 × 10^9 NWs/cm^2. Fig. 2b shows a side-view high-magnification SEM image (45° tilting) of the NWs. The top facets of the NW are square, which exhibit the expected growth habit of tetragonal crystals, while the side facets are smooth. From the cross-sectional view in Fig. S1, it can be observed that the NWs are nearly vertically aligned on the FTO substrate and the height of NWs array is around 2 μm. Compared with those NWs from other works,[13,23-24] the NWs reported here exhibit smaller average diameter and more uniform distribution on FTO substrate. It has been found that the aggregation of NWs in the previous work dramatically decreased the contact surface area at TiO$_2$/electrolyte interfaces and hence compromised the PEC device performance. In this work, the uniformly dispersed NWs show a larger surface area, and thus offer more active sites for photoelectrochemical reaction. In the second growth step, after immersed in high concentration (0.4 M) TiCl$_4$ aqueous solution, the surfaces of the NWs are decorated by TiO$_2$ seeds (Fig. S2), which is introduced according to the following reactions:[32]

TiCl$_4$ + H$_2$O → Ti(IV) complex + HCl

Ti(IV) complex → TiO$_2$

It has been reported that the presence of the seeds on the surfaces can result in a reduction in the energy barrier for TiO$_2$ nucleation.[17] A subsequent hydrothermal growth of the seeded NWs for 3 h results in densely assembled "flower"-like HNWs, as shown in Fig. 2c and 2d. The HNWs are approximately 150 nm in length and 50 nm in diameter. The final step is to grow branches on the HNWs for further increasing the roughness factor by filling out the large volume of voids in the HNW assembly. Here, TiCl$_3$ solution was used as the Ti precursors to grow nanobranches in this step. The reason was that Ti^{3+} ions need to be first oxidated to Ti^{4+} ions in an oxygen-containing aqueous solution. In this way, it would reduce the nucleation rate of TiO$_2$, resulting in the formation of TiO$_2$ nanobranches with smaller diameters. As we known, the presence of Cl$^-$ ions in the formation of NW structure was to suppress growth of the (110) faces but enhancing the growth along the (001) direction.[23] Fig. 2e and 2f show the typical SEM images of the final HHNWs, where numerous short needle-shaped hyperbranches are grown densely on the entire surfaces of the HNW backbones (cross-sectional view in Fig. S3). The hyperbranches have an average diameter and length of about 10 nm and 50 nm, respectively. The unique HHNW structure will largely improve the specific surface area
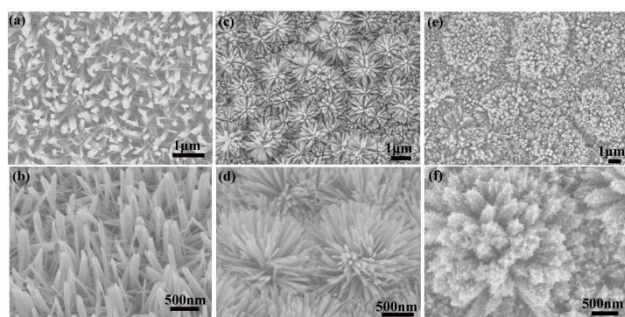
Figure 2. Top-view and side-view SEM images of (a,b) TiO$_2$ NWs, (c,d) HNWs, and (e,f) HHNWs.

and roughness factor of the nanowires.[17] The BET surface areas of the TiO$_2$ NWs, HNWs, and HHNWs are listed in Table S1. An increasing trend in the specific surface areas and roughness factor from NWs to HHNWs is evidenced, as expected.
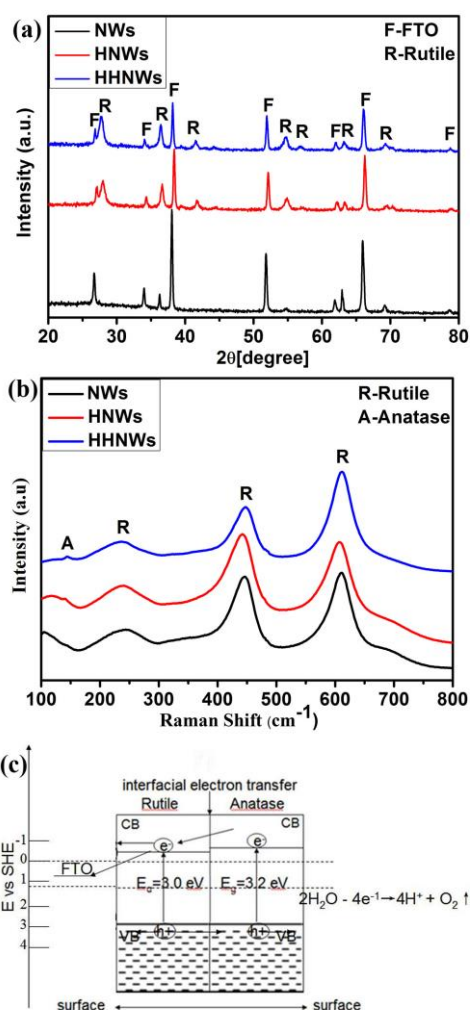

Figure 3. XRD patterns (a) and Raman spectra (b) of TiO$_2$ NWs, HNWs, and HHNWs on FTO substrates. (c) The band gap information of the three different materials (FTO, Rutile and anantase TiO$_2$).

The structure information of TiO$_2$ NWs, HNWs, and HHNWs were characterized by XRD and Raman spectra. Fig. 3a shows XRD patterns of NWs, HNWs, and HHNWs on FTO substrates. The crystal structure of all three samples can be assigned to

tetragonal rutile phase (JCPDS card No. 21-1276). The enhanced (002) peak at 2-theta of 63.20° in the bottom spectrum indicates that the NWs are well crystallized and grow preferentially along the [001] direction with the growth axis parallel to the FTO substrate. The (002) peak intensity becomes weaker in the XRD patterns of HNWs and HHNWs, which is due to that the root NWs are enclosed by non-aligned nanobranches. The three samples show similar Raman peaks associated with the lattice vibration of rutile TiO$_2$ (Fig. 3b). The three broad peaks at 237, 446, and 612 cm^{-1} can be attributed to rutile phase, which is consistent with XRD results. It should be noted that a weak peak appears at 144 cm^{-1} in the HNWs and HHNWs, but is absent in the NWs. This peak can be attributed to the characteristic vibration of anatase TiO$_2$,[37] which could be explained by the formation of a very small amount of anatase-phase nanoparticles on the rutile-phase HNWs and HHNWs when the NWs are treated with high concentration TiCl$_4$ aqueous solution. The band gap information of FTO, rutile and anatase are shown in Fig 3c. It should be noted that the existence of the anatase nanoparticles could potentially help the charge separation due to the heterojuntion band alignment effect.[38]
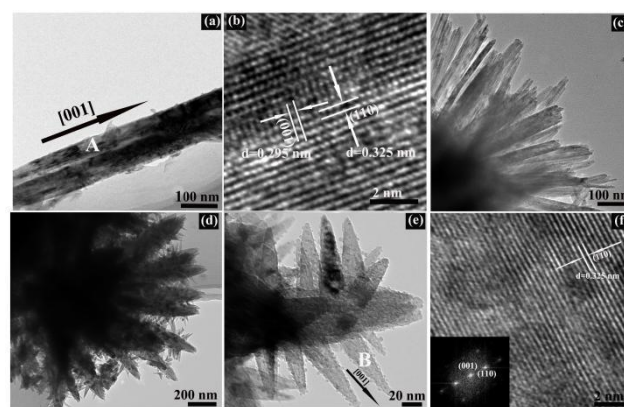

Figure 4. TEM and HRTEM images of TiO$_2$ NWs, HNWs, and HHNWs on FTO substrates. (a) TEM image of a single NW. (b) HRTEM image taken from region A in (a). (c) TEM image of a flower-like HNW assembly. (d) Low- and (e) high-maganification TEM images of the HHNW structure, (f) HRTEM image taken from region B in Fig. 4e and the SAED pattern (inset).

The morphologies and crystal structures of the NWs, HNWs, and HHNWs, have also been characterized by FE-TEM. Fig.4a shows a representative TEM image of a NW. Fig.4b shows a high-resolution TEM image taken from region A in Fig. 4a. Lattice fringes with inter-planar spacings of 0.325 nm and 0.295 nm can be index to (110) and (001) planes of the tetragonal rutile phase, respectively. The results indicate that the NW is single-crystalline tetragonal rutile phase with [001] growth direction, which is consistent with the results of TiO$_2$ NWs reported previously.[6, 23] Fig. 4c shows a typical TEM image of a flower-like HNW assembly comprising NW bundles that are developed from TiO$_2$ seeds. The TEM image in Figure 4d shows that the hyperbranches densely and uniformly grow on the surfaces of the HNWs. Close inspection of the branches (Fig. 4e) demonstrates that they grow randomly on the backbone of the HNWs and possess a surface coverage density of around 1.0×10^{11} branches/cm^2 (per unit area of NW) (Fig. 4d). Fig. 4f shows a HRTEM image of a single branch taken from region B in Fig. 4e. It shows well resolved lattice fringes, indicating good crystallinity of the branches. The corresponding selected area electron diffraction (SAED) pattern in the inset is indexed to the (110)

planes of rutile TiO_2 with a lattice constant of 0.325 nm, in the parallel direction to the length of the branch, suggesting that the branches are also single-crystalline tetragonal-rutile phase TiO_2 with the same [001] growth direction as that of the backbone. Similar flower-like TiO_2 structures were recently synthesized and used in dye-sensitized solar cells (DSSCs),[32] but our HHNWs have smaller diameters, higher surface coverage, and a lower degree of aggregation, which will be beneficial to PEC devices.
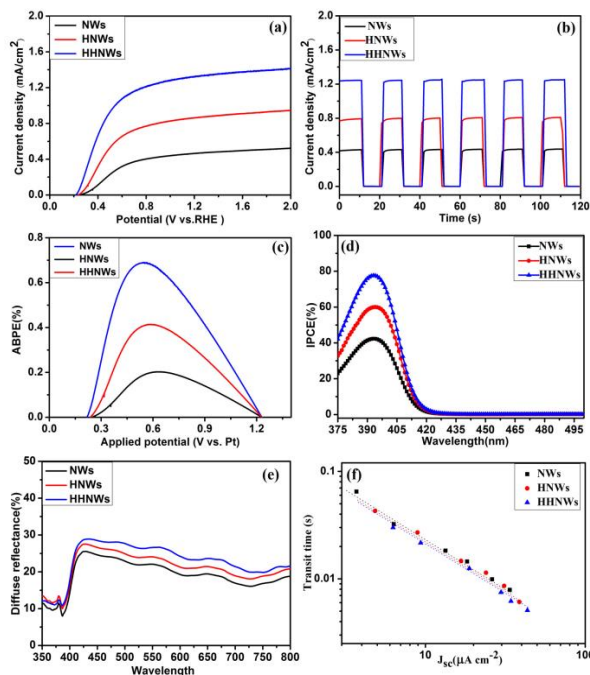

Figure 5. Photoelectrochemical properties of NWs, HNWs, and HHNWs on FTO substrates. (a) *J-V* curves measured under Xenon lamp illumination using a three-electrode setup (TiO_2 as working electrode, Pt as counter electrode, Ag/AgCl as reference electrode, scan rate of 20 mV s^{-1}. (b) Time-dependent photocurrent density at repeated 30s light on/off cycles of simulated sunlight illumination. (c) Applied bias photon-to-current efficiency (ABPE, %) of three different photoelectrodes as a function of applied potential based on the calculation method reported previously.[39] (d) IPCE measured in the wavelength range of 375−500 nm. All samples were measured at an applied bias of 1.23 V versus RHE. (e) Diffuse reflectance spectra of films of NWs, HNWs, and HHNWs grown on FTO substrates over a wavelength range of 350-800 nm. (f) The average transit time of photogenerated electrons at 1.23 V vs RHE as a function of the maximal photocurrent density for NWs, HNWs, and HHNWs grown on FTO substrates. A 385 nm LED lamp was used as the light source for the IMPS measurement.

To demonstrate the effectiveness of HHNWs for improving PEC water splitting, we compared several measurement results using TiO_2 films of three different nanostructures: NWs, HNWs, and HHNWs. One key measurement was the current density versus potential (*J-V*) under AM 1.5 G irradiation (100 mW cm^{-2}). The *J-V* curves of the TiO_2 films supported on FTO substrates were measured in 1 M NaOH using a standard three-electrode configuration. As shown in Fig. 5a, sweeping the potential anodically, the *J-V* curve of the HHNWs exhibits a sharp increase of current and reaches a prompt saturation of the photocurrent density at about 0.8 V versus RHE. The photocurrent densities of the NWs, HNWs, and HHNWs are 0.34, 0.75, and 1.21 mA cm^{-2} at 1.23 V versus RHE, respectively. The nearly 4-fold current

density increase of the HHNWs, over NWs demonstrates much higher light harvesting efficiency and largely increased contact surface area at the TiO_2/electrolyte interface of the hyperbranched hierarchical structure, which can significantly enhance PEC water splitting performance.

The chemical and structural stability during PEC water splitting is another important factor to evaluate for the potential PEC electrode materials. The corresponding transient time-dependent curves of NWs, HNWs, and HHNWs show a highly stable photocurrent density of 0.34±0.02, 0.75±0.03, and 1.21±0.03 mA cm^{-2}, respectively, at an applied bias of 1.23 V vs. RHE during 6 repeated light ON/OFF cycles (20 s duration for each cycle), as shown in Fig. 5b. It can be seen that the NWs, HNWs, and HHNWs have fast photo-response time and stable photo-stability. The dark current density remained at a very low level (<10^{-2} mA cm^{-2}) under bias potentials between 0 and 2 V, indicating the high quality of the TiO_2 crystal surfaces. Rectangular shaped photocurrent transients indicate a rapid photoresponse and a good reproducibility of the photoanodic processes.

Applied bias photon-to-current efficiencies (ABPEs) were calculated using the equation[12]

$$ABPE = \left[J_P \times \left(1.23 - \left| E_{meas} - E_{aoc} \right| \right) \frac{100}{I_0} \right]$$

where J_P is the photocurrent density, E_{meas} is the electrode potential (vs Ag/AgCl) of the working electrode at which the photocurrent was measured under illumination, and E_{aoc} is the electrode potential (vs Ag/AgCl) of the same working electrode at open circuit condition under same illumination and in the same electrolyte, and I_0 is the intensity of incident light in mW cm^{-2}.[31,38] The calculated ABPEs of the NW, HNW, and HHNW samples are plotted as a function of biasing potential as shown in Fig. 5c, where the NW and HNW samples exhibit optimal ABPEs of 0.22% at 0.61 V versus RHE and 0.43% at 0.56 V versus RHE, respectively. Impressively, a maximum efficiency of 0.71% at 0.55 V versus RHE for the HHNW sample is achieved. In addition, statistical histograms shown in Supplementary Information indicate that the photoelectrode conversion efficiency of the HHNWs is much higher than those of NWs and HNWs.

The incident photon-to-current conversion efficiency (IPCE), synonymous with external quantum efficiency (EQE), is another key parameter to evaluate the PEC materials. It can be calculated from the following equation[9]:

$$IPCE = \frac{(1240 \times I)}{\lambda \times P_{light}}$$

where I is the measured photocurrent density (mA cm^{-2}) at a specific wavelength, λ is the incident light wavelength (nm), and P_{light} (mW cm^{-2}) is the power density of monochromatic light at a specific wavelength. To further understand the overall PEC performance of the HHNW sample, IPCEs of the NW, HNW, and HHNW samples were measured at 1.23 V versus RHE as a function of incident light wavelength. As shown in Fig. 5d, the peak IPCE values of NWs, HNWs and HHNWs are 42%, 60%, and 77%, respectively, at wavelength of 375−425 nm. Such IPCE enhancement for HHNWs is presumably due to the improved surface area arising from the branched hierarchical structure. This result indicates that our HHNWs could effectively use the UV light for PEC water splitting, and the separation and transportation of photoexcited charge carriers are very efficient. Moreover, it is widely known that the enhancement of light scattering by TiO_2 photoanode films is crucial for improving the light harvesting efficiency.[40-41] To study the light scattering efficiency, the reflectivity of all three films were evaluated (Fig. 5e). As expected, the HHNWs and HNWs exhibit much higher diffuse reflectance

in the visible and near-infrared regions compared to NWs. The HHNWs shows the highest diffuse reflectance among the three films, which can be ascribed to the intrinsic optical properties of the omnidirectional, densely-packed hyperbranched nanostructure. The complicated and interconnected network architecture within the HHNWs photoelectrode could effectively multiply light absorption path length and increase the optical density, thus enable high scattering efficiency. This contributes to the elevated photocurrent density.

The charge transport behaviors in the PEC electrodes can be studied by intensity modulated photocurrent spectroscopy (IMPS),[42-43] which is also widely used in electron transport characterization of DSSCs. The average transport time for the photogenerated electrons to reach the conductive substrate, τ_d, can be derived from the IMPS measurements according to the equation: $\tau_d = 1/2\pi f_d$, where f_d is the characteristic minimum frequency of the IMPS imaginary component.[44] Fig.5f depicts τ_d of photogenerated electrons as a function of the maximal photocurrent density under an illumination of 385 nm from an LED light source. An obvious similarity in electron transport time is observed for PEC cells made of NWs, HNWs, and HHNWs, suggesting that the electrons in these hierarchical structures can transit as efficient as NWs.

Conclusions

In summary, we have successfully prepared a new photoanode architecture of hyperbranched hierarchical TiO$_2$ nanowires (HHNWs) for efficient photoelectrochemical water splitting. Compared to NWs and HNWs, the HHNWs shows significantly improved PEC performance due to enhanced light absorption and increased contact surface area at the TiO$_2$/electrolyte interface. Under solar simulator with AM 1.5 G light of 100 mW^{-2} intensity, the photocurrent densities of NWs, HNWs, and HHNWs at an applied bias of 1.23 V vs RHE are 0.34, 0.75, and 1.21 mA cm^{-2}, respectively. The highest incident photon-to-current conversion efficiencies (IPCE) obtained from our HHNWs is 77 % around 375−425 nm, which is much better than those of NWs (42 %) and HNWs (60 %) in the same UV wavelength range. We believe that the HHNWs can be used in conjunction with doping and/or dye-sensitization to further improve the PEC performance of TiO$_2$. Overall, this approach has opened a promising avenue to develop high-efficiency PEC photoelectrodes that could have substantial impacts on the PEC and photovoltaic device development.

Notes and references

[a] Department of Physics, Institute of Low-Dimensional Carbons and Device Physics, Shanghai University, Shanghai 200444, China

[b] *i*-Lab, Suzhou Institute of Nano-Tech and Nano-Bionics, Chinese Academy of Sciences, Suzhou, Jiangsu 215123, China

[+] Zhenghui Pan and Yongcai Qiu contributed equally to the work.

* E-mail: (ygzhang2012@sinano.ac.cn ; xlzhao@shu.edu.cn)

Electronic Supplementary Information (ESI) available: (1) Cross sectional SEM view of TiO$_2$ NWs; (2) SEM view of the TiO$_2$ seeded NWs; (3) Cross sectional SEM view of HHNWs; (4) statistical histograms of photoelectrode conversion efficiency are included. See DOI: 10.1039/b000000x/

1. K. Shankar, J. I. Basham, N. K. Allam, O. K. Varghese, G. K. Mor, X. J. Feng, M. Paulose, J. A.Seabold, K. S. Choi and C. A. Grimes, *J. Phys. Chem. C.* , 2009, **113**, 6327.
2. Y. Tachibana, L. Vayssieres and J. R. Durrant, *Nat. Photonics.* , 2012, **6**, 511.
3. Z. S. Li, W. J. Luo, M. L. Zhang, J. Y. Feng and Z. G. Zou, *Energy Environ. Sci.* , 2013, **6,** 347.
4. C. W. Cheng, S. K. Karuturi, L. J. Liu, J. P. Liu, H. X. Li, L. T. Su, A. L. Y. Tok and H. J. Fan, *Small*, 2012, **8**, 37.
5. Z. Zou, J.Ye, K. Sayama and H. Arakawa, *Nature*, 2001, **414**, 625.
6. I. S. Cho, Z. Chen, A. J. Forman, D. R. Kim, P. M. Rao, T. F. Jaramillo and X.L. Zheng, *Nano Lett.* 2011, **11**, 4978.
7. Y. C. Qiu, S. C. Leung, Q. P. Zhang, B. Hua, Q. F. Lin, Z. H. Wei, K. H. Tsui, Y. G. Zhang, S. H. Yang and Z. Y. Fan, *Nano Lett*. 2014, **14**, 2123.
8. N. S. Lewis and D. G. Nocera, *Natl. Acad. Sci. U.S.A.* , 2006, **103**, 15729.
9. T. Bak, J. Nowotny, M. Rekas and C. C. Sorrell, *Int. J. Hydrog. Energy.* , 2002, **27**, 991.
10. M. G. Walter, E. L. Warren, J. R. McKone, S. W. Boettcher, Q. X. Mi, E. A. Santori and N. S. Lewis, *Chem. Rev.* , 2010, **110**, 6446.
11. A. Fujishima and K. Honda, *Nature* 1972, **238**, 37.
12. U. M. Shahed, A. S. Mofareh and W. B. Ingler, *Science*, 2002, **297**, 2243.
13. Y. C. Pu, G. M. Wang, K. D. Chang, Y. C. Ling, Y. K. Lin, B. C. Fitzmorris, C. M. Liu, X. H. Lu, Y. X. Tong, J. Z. Zhang, Y. J. Hsu and Y. Li, *Nano Lett.* 2013, **13**, 3817.
14. S. C. Warren and E. Thimsen, *Energy Environ. Sci.* ,2011, **9**, 5133.
15. 15 Z. H. Zhang, L. B. Zhang, M. N. Hedhili, H. N. Zhang and P. Wang, *Nano Lett,* 2013, **13**, 14.
16. W. Chen, Y. C. Qiu and S. H. Yang, *Phys. Chem. Chem. Phys.* , 2012, **14**, 10872.
17. Y. C. Qiu, K. Y. Yan, H, Deng and S. H. Yang, *Nano Lett*. 2012, **12**, 407.
18. Y. S. Hu, A. K. Shwarsctein, A. J. Forman, D. Hazen, J. N. Park and E. W. McFarl, *J. Mater. Chem.* , 2008, **20**, 3803.
19. S. J. Hong, S. Lee and J. S. Jang, *Energy Environ. Sci.* , 2011, **4**, 1781.
20. X. W. Wang, G. Liu, G. Q. Lu and H. M. Cheng, *Int. J. Hydrogen. Energ.* , 2010, **35**, 8199.
21. M. Frites and S. U. M. Khan, *Electrochem. Commun.* 2009, **11**, 2257.
22. A. S. Nair, Z. Peining, V. J. Babu, Y. S. Yuan and S. Ramakrishna, *Phys. Chem. Chem. Phys.* , 2011, **13**, 21248.
23. X. J. Feng, K. Shankar, O. K. Varghese, M. Paulose,T. J. Latempa and C. A.Grimes, *Nano Lett.* 2008, **8**, 3781.
24. M. Xu, P. Da, H. Wu, D. Zhao and G. Zheng, *Nano Lett.* 2012, **12**, 1503.
25. G. Wang, H. Wang, Y. Ling, Y. Tang, X. Yang, R. C. Fitzmorris, C. Wang, J. Z. Zhang and Y. Li, *Nano Lett.* 2011, **11**, 3026.
26. G. K. Mor, K. Shankar, M. Paulose, O. K. Varghese and C. A. Grimes, *Nano Lett.* 2005, **5**, 191.
27. Y. B. Liu, J. H. Li, B. X. Zhou, H. C. Chen, Z. S. Wang and W. M. Cai, *Chem. Commun.*2011, **47**, 10314.
28. M. J. Bierman and S. Jin, *Energy Environ. Sci.* , 2009, **2**, 1050.

29. I. Herman, J. Yeo, S. Hong, D. Lee, K. H. Nam, J. Choi, W. Hong, C. P. Grigoropoulos and S. H. Ko, *Nanotechnology,* 2012, **23**, 194005.

30. S. H. Ko, D. Lee, H. W. Kang, K. H. Nam, J. Y. Yeo, S. J. Hong, C. P. Grigoropoulos and H. J. Sung, *Nano Lett.*, 2011, **11**, 666.

31. J. Shi, Y. Hara, C. L. Sun, M. A. Anderson and X. D. Wang, *Nano Lett.* 2011, **11**, 3413.

32. D. Lee, Y. Rho, F. I. Allen, A. M. Minor, S. H. Ko and C. P. Grigoropoulos, *Nanoscale,* 2013, **5**, 11147.

33. G. S. Wu, J. P. Wang, D. F. Thomas and A. Chen, *Langmuir* 2008, **24**, 3503.

34. W. Q. Wu, Y. F. Xu, H. S. Rao, C. Y. Su and D. B. Kuang, *J. Am. Chem. Soc.* , 2014, **136**, 6437.

35. Wu. Q. Wu, H. L. Feng, H. S. Rao, Y. F. Xu, D. B. Kuang and C. Y. Su, *Nat. Commun.* , 2014, **5**, 3968.

36. W. N. Ren, H. F. Zhang, D. Z. Kong, B. Liu, Y. P. Yang and C. W. Cheng, *Phys. Chem. Chem. Phys.* , 2014, **16**, 22953.

37. N.G. Park, G. Schlichtho1rl, J. V. D. Lagemaat, H. M. Cheong, A. Mascarenhas and A. J. Frank, *J. Phys. Chem. B.* , 1999, **103**, 3308.

38. M. G. Walter, E. L. Warren, J. R. McKone, S. W. Boettcher, Q. Mi, E. A. Santori, and N. S. Lewis, *Chem. Rev.* , 2010, **110**, 6446.

39. V. E. Ferry, L. A. Sweatlock, D. Pacifici and H. A. Atwater, *Nano Lett.*, 2008, **8**, 4391.

40. D. H. Chen, F. Z. Huang, Y. B. Cheng and R. A. Caruso, *Adv. Mater.*, 2009, **21**, 2206.

41. Y. C. Qiu, W. Chen and S. H. Yang, *Angew. Chem. Int. Ed*, 2010, **49**,3675.

42. K. Zhu, N. R. Neale, A. Miedaner and A. J. Frank, *Nano Lett*, 2007, **7**, 69.

43. H. X. Wang, P. G. Nicholson, L. Peter, S. M. Zakeeruddin and M. Gr¨atzel, *J. Phys. Chem. C.* , 2010, **114**, 14300.

44. K. Fan, J. N. Chen, F. Yang and T. J. Peng, *Mater. Chem.* 2012, **22**, 4681.

Synthesis of three-dimensional hyperbranched TiO$_2$ nanowire arrays with significantly enhanced photoelectrochemical hydrogen production

Zhenghui Pan,[a,b,+] Yongcai Qiu,[b,+] Jie Yang,[a] Alagesan Subramanian,[b] Wanfei Li,[b] Meinan Liu,[b] Lisha Zhou,[b] Yijun Xu,[b] Leimei Sheng,[a] Xinluo Zhao*[a], and Yuegang Zhang*[b]